Method of Atmospheric Density Measurements During Shuttle Entry Using Ultraviolet-Laser Rayleigh Scattering

Robert L. McKenzie*
NASA Ames Research Center, Moffett Field, California

An analytical study and its experimental verification are described that show the performance capabilities and hardware requirements of a method for measuring atmospheric density along the Space Shuttle flight path during entry. Using onboard instrumentation, the technique relies on Rayleigh scattering of light from a pulsed ArF excimer laser operating at a wavelength of 193 nm. The method is shown to be capable of providing density measurements with an uncertainty of less than 1% and with a spatial resolution along the flight path of 1 km, over an altitude range of 50–90 km. Experimental verification of the signal linearity and the expected signal-to-noise ratios is demonstrated in a simulation facility at conditions duplicating the signal levels of the flight environment.

Nomenclature

A_c = entrance aperture area of the collection optics
A_L = laser beam cross-sectional area
c = speed of light
d_p = primary mirror diameter
d_s = secondary mirror diameter
E_L = laser pulse energy
h = Planck's constant
I_{filter} = solar flux (photons/cm^2·s) transmitted by the filter
n_p = aerosol particle refractive index
n_{pulse} = number of accumulated pulses
n_{stp} = refractive index of air at standard temperature and pressure
N_{stp} = number density of standard temperature and pressure
$\bar{N}_{\text{atm}}$ = locally averaged atmospheric number density
$\bar{N}_p$ = aerosol particle total number density
N_{phot} = rms noise amplitude (photoelectrons)
N_r = aerosol particle number density in the radius range, r to $r+dr$
P_L = incident laser power
P_s = power of Rayleigh-scattered light
r = aerosol particle radius
R_{solar} = fraction of solar flux scattered by the atmosphere from the horizon
SNR = signal-to-noise ratio
S_{part} = aerosol particle scattering signal (photoelectrons)
S_{Ray} = single-pulse Rayleigh signal (photoelectrons)
S_{solar} = solar background signal (photoelectrons)
V = volume
x = position along the laser beam measured outward
x_0 = minimum observation range
ΔN_{atm} = rms uncertainty in atmospheric number density measurement
Δt = signal integration period
η = combined photoelectron production efficiency
λ = wavelength
ρ_n = depolarization ratio
σ_0 = Rayleigh cross section as defined by Eq. (3)
σ_p = average particle scattering cross section
Ψ = azimuthal scattering angle
Ω_c = collection optics solid angle

Received March 14, 1988; revision received Aug. 1, 1988.

*Research Scientist. Associate Fellow AIAA.

Introduction

OVER the altitude range of 50–100 km, where the Space Shuttle is at an angle of attack for maximum aerodynamic braking, meteorological fluctuations in the atmosphere density are also their greatest. As Fig. 1 shows, unpredictable departures from the 1976 Standard Atmosphere[1] may reach extremes as large as 80% with a 1% probability. Disturbances evaluated from radiosonde data[2–4] show the presence of discrete layers of turbulence having a minimum thickness of tens of meters and vertical wavelengths of about 1 km. Similar results have been derived from accelerometer data taken during the first 12 Shuttle flights.[5] Those data indicate that the flights encountered extreme density variations from −55 to +10% at altitudes of 80−100 km and abrupt density changes of 15−20% over vertical distances of less than 1 km.

The uncertainty with which these ambient density variations are measured along the entry flight path can directly affect the evaluation of the Shuttle's aerodynamic coefficients from dynamic flight data. The density uncertainties can obscure the contributions of such factors as real-gas effects and full-scale viscous effects that influence the aerodynamic coefficients in flight, but are not accurately represented in wind-tunnel measurements. Moreover, in the low-density transition regime between free-molecule and continuum flow, even the ratios of forces such as lift to drag are density dependent. For Shuttle trajectories, this transition regime occurs in the 80–140 km altitude range.[6]

At present, determinations of upper atmosphere densities along the flight path of the Shuttle are obtained by a variety of methods including measurements by radiosondes and rocket-launched meteorological spheres,[7] by accelerometer data taken from instruments on board the Shuttle and used in combination with radiosondes and other flight data,[6,8] and by instrumentation that samples air data from the surface of the vehicle.[9–11] The methods are summarized in Table 1 along with estimates of their uncertainty in the determination of density over the altitude range of their applicability.

None of the methods currently available is able to measure density along the flight path both directly and at the time of flight. Only the radiosondes and rocketsondes provide a direct measurement of density, but the results must be extrapolated to the time and location of the entry vehicle flight path.[7] Best-estimated trajectories (BET) are obtained by combining onboard inertial measurement unit (IMU) accelerometer data with radiosonde data,[8] but the use of IMU/BET to imply values of atmospheric density also requires a detailed and accurate knowledge of the vehicle aerodynamic force coefficients at the particular flight speed, angle of attack, and control surface configuration for each point along the trajectory. For example, the 3–5% density uncertainty shown in Table 1 for the IMU/BET determinations reflects the magnitude of an apparent variation from the standard normal-force coefficients given by the Orbiter aerodynamic data base.[5]

To date, the most accurate determination of atmospheric density obtained from flight data in the continuum flow regime has come from the Shuttle entry air data system (SEADS).[9,10] It measures pressures on the nose of the airframe using an array of surface orifices. An analysis of the data relies on an independent knowledge of the aerodynamics of the nose flow and leads to determinations of the dynamic pressure and the angle of attack with uncertainties of 3% and 0.3 deg, respectively.[12] Although dynamic pressure is the primary variable of interest for the determination of aerodynamic force coefficients, atmospehric density has also been extracted from the data with an uncertainty of 3–4%.

Table 1 also includes onboard instrumentation giving atmospheric densities at higher altitudes where low-density flow effects are prevalent.[6,11] However, much greater uncertainties accompany the results and are again partly a consequence of the uncertainty in aerodynamic force coefficients.

In this paper, the performance capabilities and the hardware requirements are described for a technique in which atmospheric density along the Shuttle flight path is measured using onboard laser-based instrumentation. The principal objectives are to provide direct and more accurate measurements of atmospheric density, over a maximum range of altitudes including those where the greatest meteorological variations in the atmosphere occur.

The introduction of laser-based instrumentation on board the Shuttle will also lay the foundation for more advanced measurements within the shock layer, in support of aerothermodynamic studies and computer model verification for advanced entry vehicle design. The feasibility of such measurements based on current technology is discussed in Ref. 13 for several extensions to this concept. They provide density profiles within the shock layer during entry, using the same laser system described here for atmospheric density measurements.

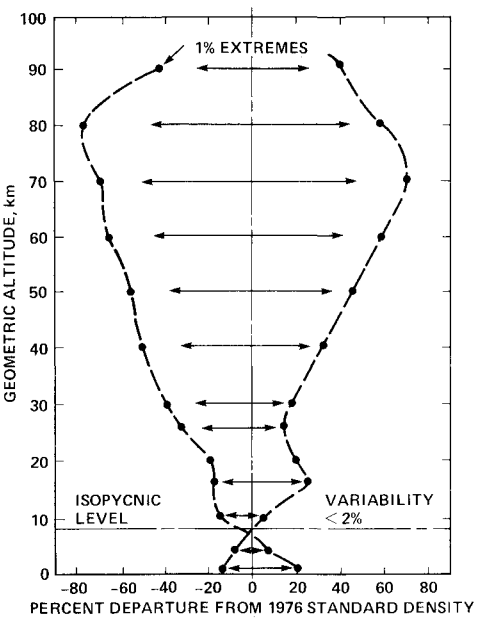

Fig. 1 Variability of density from the *U.S. Standard Atmosphere, 1976*,[1] (extremes amplitudes shown are those occurring with 1% probability).

Table 1 Methods of atmospheric density determination along the Space Shuttle flight path

Instrument[a]	Type/Ref.	Primary objective	Altitude range, km	Density uncertainty, %	Comments
Radiosonde/ LAIRS	Rocket-launched probes, spheres[7]	Upper atmosphere temperature and density	30–90	3–5	Data not on flight path nor taken at time of flight
IMU/BET	Three-axis accelerometers[8]	Vehicle dynamics	0–90	3–5	Depends on known aerodynamic coefficients
SEADS	Pressure orifices in Shuttle nose[9,10]	Freestream dynamic pressure, angle of attack	0–95	3–4	Currently most accurate air data instrumentation
SUMS	Mass spectrometer[11]	Freestream density, gas composition	90–130	10–20	Only instrument with capability in rarefied flight regime
HiRAP	Very-low-level accelerometers[6]	Vehicle dynamics in low-density regime	90–160	5–20	Used in conjunction with SUMS for high-altitude density determination
This method	UV Rayleigh scattering	Freestream density	50–90	<1	Independent of other flight or atmosphere data

[a]BET = best estimated trajectory (data analysis procedure), HiRAP = High resolution accelerometer package, IMU = inertial measurements unit, LAIRS = Langley atmosphere information retrieval system (computer code), SEADS = Shuttle entry air data system, SUMS = Shuttle upper atmosphere mass spectrometer.

Concept

This technique relies on the Rayleigh scattering of light from a pulsed ultraviolet laser. The laser beam emerges from the window in the middeck crew hatch and propagates in a direction that is nearly normal to the longitudinal body axis of the vehicle. Light scattered backward by the ambient air is collected during each pulse by optics attached to the inside of the window. The collection optics are arranged so that only light scattered from the length of the beam beyond the shock layer is detected. The intensity of the scattered light is time integrated over a selected period following each laser pulse to obtain a signal that is a measure of the total energy of light scattered during that period. The signal, which is normalized by the laser pulse energy, is linearly proportional to the atmospheric density in the observed length of the beam and has no significant dependence on any other properties of the atmosphere or on the flight conditions.

Requirements and Limiting Factors

To establish the altitude and spatial-resolution requirements for these measurements, the radiosonde[2-4] data and the Shuttle flight data[5] show that altitudes at least up to 80 km must be included if the largest density variations are to be detected. To encompass the low-density flight regime, altitudes to 100 km would be preferred. The data also suggest that a spatial resolution of 1 km or less is required to adequately define the small-scale structure that has been observed. Finally, a measurement uncertainty of less than 1% is selected as a goal that will insure an adequate resolution of the Shuttle aerodynamic coefficients from flight data and emphasize the improved capabilities of this method when compared to present methods.

The uncertainty of an optical measurement is usually characterized by its overall signal-to-noise ratio (SNR). If $\bar{N}_{atm}$ denotes the local atmospheric number density averaged over the temporal or spatial interval of its measurement and ΔN_{atm} is the rms standard deviation (uncertainty) in the measurement, then the relative uncertainty of the measurement is $\Delta N_{atm}/\bar{N}_{atm}$ and the overall SNR is defined by

$$\text{SNR} = \bar{N}_{atm}/\Delta N_{atm} \tag{1}$$

Thus, to obtain an uncertainty of less than 1%, the SNR must be greater than 100.

The uncertainty in the measurement arises, in part, from photon-statistical noise that is an unavoidable feature of any photodetection process. It is equal to the square root of the total number of photoelectrons produced in the detector from all sources during a measurement time interval. Possible contributing light sources, in addition to the Rayleigh-scattered light, include direct sunlight and sunlight scattered by the atmosphere, cloud tops, and Earth's surface albedo. A further contributor to the measurement uncertainty is the scattering of laser light from aerosols and dust in the atmosphere. Such scattering is indistinguishable from Rayleigh scattering and must be included both as a component to the photon-statistical noise and as an uncertainty in the determination of atmospheric density that is derived from the total signal.

Since the measurement uncertainty is related to the total number of photoelectrons accumulated during a measurement interval, the signal is most conveniently described in the same way. Hence, the total signal is defined as equal to the total number of photoelectrons detected during a measurement interval. To separate the Rayleigh contribution from the total signal, the flight instrumentation must include a separate measurement of the continuous background light, made in a time interval between laser pulses when no Rayleigh scattering is present. This measurement can be made using simple electronic gating of the signal from the same photodetector used to observe the Rayleigh signal.

Because the photon-statistical noise increases only as the square root of the total signal, the SNR increases as the Rayleigh signal increases. The Rayleigh signal can be maximized both by increasing the Rayleigh-scattered light produced by a single laser pulse and by summing the single-pulse signals over a number of pulses. Since the number of accumulated pulses will be limited to the number occurring within the time that is necessary to travel a specified distance along the flight path, the specified spatial resolution along the flight path will limit the SNR and encourage the use of a high-average-power laser.

Instrumentation Design

Rayleigh Scattering

The use of Rayleigh scattering is attractive because it is the simplest of all radiative interactions with gases. The scattered light is at nearly the same wavelength and bandwidth as the source, its intensity is proportional to the number density of the medium, but it is insensitive to the temperature of the medium. The cross section for Rayleigh scattering is strongly dependent on wavelength, but, in the case of backward scattering from gases, the intensity of scattered light is independent of the polarization of the incident light. Furthermore, in air at ambient temperatures, the photon yield for Rayleigh scattering is greater than that from any other radiative interaction, including laser-induced fluorescence. Thus, the optical signal is maximum, while the requirements on the laser energy and its spectral qualities are minimum.

The magnitude of the Rayleigh signal can be related to the physical properties of the laser and to the parameters of the collection optics by first describing the power of light scattered in the backward direction from a volume V into an element of solid angle $d\Omega$. The result is[14]

$$\frac{\partial P_s}{\partial \Omega} = \frac{P_L}{A_L} \bar{N}_{atm} V \left(\frac{2}{2+\rho_n}\right) \frac{\partial \sigma}{\partial \Omega} \tag{2}$$

For most gases, the depolarization factor ρ_n is typically very small compared to unity[15] ($\rho_n = 0.02$ for N_2 and 0.06 for O_2). Hence, for this application, the term in parentheses is assumed equal to unity.

The differential Rayleigh cross section $\partial\sigma/\partial\Omega$ varies with the scattering direction according to

$$\frac{\partial \sigma}{\partial \Omega} = \sigma_0 \frac{1}{2}(1 + \cos^2\psi) \tag{3}$$

Thus, for backward scattering, the azimuthal scattering angle $\psi = 180$ deg and $\partial\sigma/\partial\Omega = \sigma_0$. The coefficient σ_0, which is frequently referred to as the Rayleigh cross section, varies with wavelength λ according to

$$\sigma_0 = \frac{4\pi^2}{\lambda^4}\left(\frac{n_{stp}-1}{N_{stp}}\right)^2 \tag{4}$$

Corrections to Eq. (4) to account for variations of the term $(n_{stp}-1)/N_{stp}$ with temperature can be shown to be negligible for this application.[16]

The effects of ultraviolet resonances on the Rayleigh cross section are also a consideration, particularly for O_2, which has absorption transitions that fall within the bandwidth of the ArF laser centered at 193 nm. Dispersion data for air, which define the variation of refractive index with wavelength and can be related to the Rayleigh cross section, show no significant resonant effects at ultraviolet wavelengths down to 185 nm.[17] That conclusion is supported further by calculations[18]

based on recent values of the oscillator strengths[19,20] for O_2, which indicate that the resonance enhancement should be much less than 1%. Consequently, the cross-section measurements reported in Ref. 15 for O_2 and N_2 at wavelengths down to 364 nm have been used to compute a cross-section parameter for air (79% N_2, 21% O_2) of $\lambda^4\sigma_0 = 4.81\times10^{-17}$ nm$^4\cdot$cm^2.

The effects of optical absorption for wavelengths in the ArF laser bandwidth centered at 193 nm are also found to be negligible for the range of densities considered in this application. Consequently, the atmosphere may be considered to be optically thin for this analysis. Because the absorption is due to individual rotational features in the Schumann-Runge bands of oxygen, not all wavelengths in the laser bandwidth are absorbed and the absorption depth does not behave according to Beer's law. However, the effective optical depth at room conditions is approximately 5 m and it becomes much longer than the observed path length at densities corresponding to an altitude of 50 km. The maximum density for which air may be assumed to be optically thin for this application has been determined experimentally and will be described in a following section.

For pulsed applications in an optically thin gas, the Rayleigh signal may be evaluated by integrating Eq. (2) over the solid angle $\Omega(x)$ observed from each position x along the laser beam and over the duration of the signal pulse. It may also be divided by the energy per photon hc/λ to cast the expression in terms of the total number of scattered photons per pulse. The single-pulse Rayleigh signal S_{Ray} is then obtained by multiplying by the quantum efficiency of the photodetector and by the efficiency of the collection optics. Both efficiencies are combined into the parameter η. The result is

$$S_{Ray} = \frac{\lambda}{hc}\sigma_0 \bar{N}_{atm} E_L \eta \int \Omega(x)\,dx \tag{5}$$

Optical Configuration

The Rayleigh signal is maximized by observing the greatest length of laser beam possible. A coaxial Cassegrain arrangement of the type shown in Fig. 2 accomplishes that objective by collecting backscattered light from the entire beam that propagates beyond the range-limiting ray. The coaxial arrangement also eliminates the need for any critical alignment with the laser beam and, with perfect alignment, it rejects all of the scattered light from within the shock layer.

The relevant parameters of the collection optics are the diameters of the mirrors and the point x_0 on the laser beam which is intersected by the range-limiting ray. The clear aperture area of the collection optics is then $A_c = (d_p^2 - d_s^2)\pi/4$ and the solid angle for light collection from x to $x + dx$ can be accurately approximated by $\Omega(x) \approx A_c/x^2$ for all values of x where $4x^2/d_p^2 \gg 1$. Equation (5) may then be integrated from $x = x_0$ to ∞ with the result

$$S_{Ray} = \frac{\lambda}{hc}\sigma_0 \bar{N}_{atm} E_L \eta \frac{A_c}{x_0} \tag{6}$$

Values of the minimum range x_0 are dictated by the Shuttle flowfield. While the vehicle is in hypersonic flight (Mach no. >5, altitude >40 km) the maximum shock layer thickness in the direction of the laser beam is estimated to be less than 200 cm.[21-23] Hence, this design is based on $x_0 = 200$ cm. The remainder of the collection optics design is determined by the size of the crew-hatch window, which limits the entrance aperture diameter to $d_p = 23$ cm.

Figure 2 also shows the crew-hatch window to have three panes. Note that the laser beam is transmitted through separate central windows in each pane, which are optically isolated from the outer segments by a beam tube. This configuration was found to be essential to eliminate the large signals caused by Rayleigh-scattered light from the window material that would travel radially outward within the window and scatter into the collection optics.

As a consequence of the foregoing constraints, the collection optics have a total collection efficiency of 35%, including absorption by the window material and reflection losses from their surfaces, but not including the quantum efficiency of the photodetector. The laboratory version had an overall length of 40 cm, including the detector housing and the mirror mounts.

Laser Selection

The relevant parameter defining the laser performance for this application is its average power. Pulsed lasers are generally superior to continuous-wave lasers for obtaining high average power, particularly in the ultraviolet spectral regions. Hence, they are the primary candidates for this application.

The major factors contributing to the selection of a laser are illustrated in Fig. 3. For example, by combining Eqs. (4) and (5), the wavelength dependence of the Rayleigh signal can be shown to be proportional to $1/\lambda^3$ when the signal is described in terms of photoelectrons per pulse. This feature of Rayleigh scattering is shown by Fig. 3 to encourage the use of the shortest wavelength possible. Further encouragement is given by the rapid decrease in solar radiation with wavelength in the ultraviolet spectral region, also shown in Fig. 3. On the other

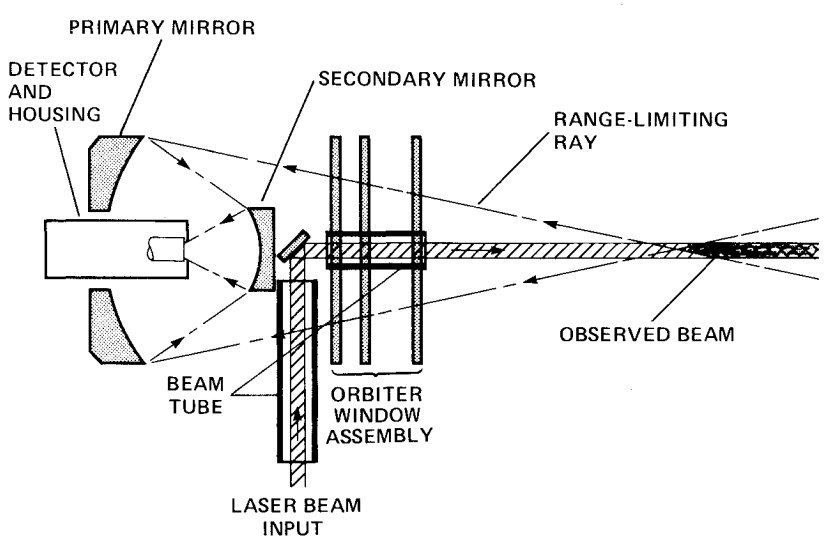

Fig. 2 Configuration of laser transmitter optics and scattered-light collection optics that would be mounted on the interior of the crew hatch window on the Shuttle middeck.

hand a practical lower limit in wavelength is dictated by the radiative absorption of the window material, as shown in Fig. 3 by the transmission curve for uv-grade fused silica.

The wavelengths of two ultraviolet lasers are also indicated in Fig. 3. They represent the choices having the shortest acceptable wavelengths that can be obtained from current laser technology with comparatively high average power.

The ArF excimer laser, operating at 193 nm, is most ideal because its wavelength falls closest to the window transmission limit. Commercial units are available[24] that can provide repetition rates exceeding 200 Hz and pulse energies exceeding 200 mJ, thereby giving average powers reaching 60 W. On the other hand, the laser and its power supply is typically large (150 cm long) and heavy (250 kg). Moreover, it requires high electrical power (1-3 kW) and relies on toxic gases (fluorine).

The second candidate, a frequency-quadrupled Nd:YAG solid-state laser operating at 266 nm, is commercially available with sizes and weights that are smaller than most excimer lasers and it requires no gases. However, the electrical power requirements for the currently available flash-lamp-excited versions can be equally large. Unfortunately, commercial Nd:YAG lasers operating at 266 nm are typically limited to pulse energies up to 20 mJ and to repetition rates up to 30 Hz, thereby giving maximum average powers up to only 0.6 W. Nevertheless, consideration of the Nd:YAG laser for this application is compelling because its installation in the Shuttle would be less imposing.

Lasers operating at longer wavelengths, with greater average powers than either of the two choices above, were found not to be competitive because of the smaller SNR resulting from a smaller Rayleigh cross section in combination with a larger solar background and particle scattering signal.

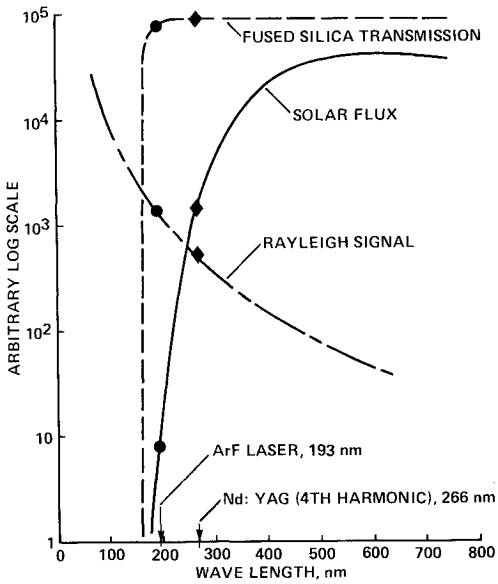

Fig. 3 Wavelength dependence of factors affecting the measurement performance (symbols mark the wavelengths at 193 and 266 nm of the two lasers evaluated).

Table 2 Detector characteristics

Photomultiplier tube
Photocathode material: CsTe on uv fused silica
Quantum efficiency: 15% from $\lambda = 193$-266 nm
Rise time: 0.7 ns
Minimum gain: 1×10^3 at 800 V
Maximum gain: 2×10^6 at 3500 V
Maximum peak anode current: 20 mA
Maximum average anode current: 0.2 mA
Filter
Peak transmission: 16%
Bandpass: 22nm (FWHM)

Performance

The remaining factors influencing instrument performance include the detector characteristics, signal integration period, intensity of the solar background, and competition with the Rayleigh signal by particle scattering. In the paragraphs to follow, each of these factors is evaluated and then combined into an overall SNR expression.

Detector Characteristics

The parameters used here that characterize the photodetector are modeled after an eight-stage photomultiplier with a CsTe solar-blind photocathode. The spectral response of the photosurface corresponds to a quantum efficiency of 15% over the wavelength range of 193-266 nm. An optical interference filter with its bandpass centered on the laser wavelength is also incorporated to reduce the photon-statistical noise contributed by the solar background. The relevant electrical features of the photomultiplier tube (PMT) and the filter parameters are summarized in Table 2.

Signal Integration

The time-dependent Rayleigh-signal waveform depends on the position x of the outward propagating laser pulse and decreases as $1/x^2$. The time-integrated signal is maximized by integrating the waveform over a period that extends to infinity, as was done to obtain Eq. (5). However, continuous solar background radiation also reaches the detector during the same integration period and contributes to the accumulated photon-statistical noise. Consequently, the integration period should be terminated before the integral has reached its full value.

In addition, light that is multiply scattered by particles and optical surfaces at close range is never completely rejected by the Cassegrain optical arrangement. To eliminate the risk of such spurious signals, the integration period is not started until after the tail of the laser pulse has cleared x_0.

Detailed calculations have been performed that simulate the time-dependent waveform of the Rayleigh scattering signal. The results show that if the integration period is started after the time at which the entire 16 ns laser pulse is beyond x_0 and is continued to the time when 90% of the remaining integral has been received, the integration period is $\Delta t = 80$ ns and the acquired integral is 54% of the value obtained by integrating over all time. This feature is included in the performance calculations to follow, as a conservative measure.

Solar Background

The contributions to solar background that are considered in this application correspond to flight maneuvers in which the Shuttle is either rolled to a position where the sun is directly in view of the collection optics, one in which the field of view is downward and filled entirely by the Earth's surface, or one in which the horizon is in view and the sun is behind the observer. In the latter two cases, the background will include the light scattered by the atmosphere. The background signal in all cases is proportional to the solar flux transmitted by the detector filter. For these calculations, the solar flux was taken from the solar spectral irradiance standard curve[25] and convolved with a filter transmission curve centered at each laser wavelength.

For a filter bandpass centered at 193 nm, in which the transmitted solar flux is smallest, direct observation of the sun was found to produce a continuous signal that exceeds the maximum average anode current of the PMT by several orders of magnitude. Hence, direct solar observation must always be avoided. That can be accomplished easily by including a small

shutter in front of the PMT that closes when the image of the sun approaches the edge of the detector aperture.

To evaluate the background signals for a downward or horizontal-looking position, radiance values for solar scattering in a backward direction by the atmosphere are taken from Monte Carlo calculations[26] for wavelengths down to 270 nm. The calculations include the effects of ozone absorption, multiple scattering including Rayleigh and aerosol contributions, and surface albedo. The results show that, for wavelengths below 300 nm, ozone absorption is the largest contributor to the loss of incident solar irradiance and its subsequent scattering. As a consequence, solar light at those wavelengths does not reach the lower atmosphere, cloud tops, or Earth's surface. The scattering intensity in all directions is then independent of cloud or surface albedo. The calculations also show that the scattered radiance is dominated by Rayleigh scattering and that it can be 2–10 times larger from the horizon than from the nadir, depending on the position of the sun. At a wavelength of 270 nm, the maximum fraction of solar flux appearing as scattered radiance from the horizon is estimated to be $R_{\text{solar}} = 2 \times 10^{-4}$. Since ozone absorption decreases when going from 270 to 193 nm and the Rayleigh cross section increases, the two effects combine to imply a larger value of R_{solar} at 193 nm. However, in the absence of a complete calculation, the same fraction was assumed for both wavelengths.

The solar flux is also assumed to be backscattered uniformly into 2π sr. Moreover, for a solar background in which no contribution from surface scattering occurs, altitude is not a relevant parameter. The scattered light appears to come from an extended field. It fills the field of view determined by its corresponding solid angle Ω_c. The effective area through which light entering the collection optics passes is then that of the spherical-cap area described by $A_c/(1-\Omega_c/4\pi)$ and the solar background signal may be evaluated by

$$S_{\text{solar}} = I_{\text{filter}} R_{\text{solar}} \Delta t \eta \frac{A_c}{1-\Omega_c/4\pi} \tag{7}$$

For the optical system used here, $A_c = 308$ cm and $\Omega_c/4\pi = (d_p/4x_0)^2 = 8.3 \times 10^{-4}$.

Calculations using Eq. (7) show that, while the solar background at $\lambda = 193$ nm is not expected to be large, it becomes a significant contributor to the measurement uncertainty at $\lambda = 266$ nm.

Particle Scattering

At lower altitudes, the competition of particle scattering with the Rayleigh scattering becomes the major factor contributing to the uncertainty. It thereby limits the lowest altitude at which this concept can be applied. Unfortunately, an estimation of scattering by atmospheric particles is a complex problem that is not predicted as accurately as it is for gaseous Rayleigh scattering. Furthermore, most of the detailed studies of atmospheric particle scattering have been confined to altitudes below 30 km where it is most significant. Therefore, to estimate the effects of particle scattering at altitudes up to 100 km, an approach has been taken for determining the average scattering cross section that is very approximate, even though it includes realistic models for the particle size distribution and for the particle density variations with altitude.

To that end, the signal owing to particle scattering may also be described by Eq. (6) except that the Rayleigh cross section is replaced by an average particle cross section that depends on the distribution of particle sizes. The expressions used here for the cross sections pertain to the total amount of light scattered into 4π sr. Since the intensity of light scattered by particles in the backward direction is known to be 10^{-3}–10^{-1} of the intensity in the forward direction,[27] the total cross sections used here are a closer representation of the forward-scattered intensity and should lead to an overprediction of the backscattering. On the other hand, these arguments pertain to single-particle scattering. The degree of overprediction is expected to be offset somewhat by the opposite effects of multiple scattering, which will redirect some to the light that is scattered forward into the backward direction.

To estimate the average particle scattering cross section, the total scattering cross section for transparent spherical particles with a radius much smaller than λ (i.e., $2\pi r/\lambda \ll 1$), is given by[27]

$$\sigma_p' = \frac{8}{3}\left(\frac{n_p^2-1}{n_p^2+2}\right)^2\left(\frac{2\pi r}{\lambda}\right)^4 \pi r^2 \tag{8}$$

Experimental refractive index data for aerosols at infrared wavelengths[28,29] show that $n_p = 1.5$ is a representative value. For large particles where $2\pi r/\lambda \gg 1$, the effective particle total cross section is nearly independent of λ and may be approximated by[27]

$$\sigma_p'' = 2\pi r^2 \tag{9}$$

The average particle cross section for a distribution of particle sizes is then estimated for a given wavelength by

$$\sigma_p = \frac{1}{\bar{N}_p}\int_0^\infty N_r(r)\sigma(r,\lambda)dr \tag{10}$$

where the cross section to be used in the integral is the smaller of the two values obtained from Eqs. (8) and (9).

The size distribution given by the haze model C proposed by Deirmendjian[30] and slightly modified[28] has been used here to obtain $\sigma_p = 7.2 \times 10^{-10}$ cm^2 for both $\lambda = 193$ and 266 nm. The cross section is insensitive to wavelength in the ultraviolet spectrum because it is dominated by particle sizes where $2\pi r/\lambda \gg 1$. Haze model C is assumed to be representative of particle distributions at all altitudes from sea level to 100 km, excluding meteoric material having a radius of less than 0.1 μm.[31] Since the average cross section used here is insensitive to scattering from such small particles, it is assumed to be applicable to all altitudes for the wavelengths considered.

The ratio of the signal contributed by particle scattering to that from Rayleigh scattering is then simply

$$S_{\text{part}}/S_{\text{Ray}} = \bar{N}_p\sigma_p/\bar{N}_{\text{atm}}\sigma_0 \tag{11}$$

It is independent of all instrument parameters other than wavelength and it is a measure of the uncertainty in the density measurement caused by particle scattering.

Values of the signal ratio given by Eq. (11) were calculated using a recommended model[28] for the total particle densities at altitudes from sea level to 100 km and for $\lambda = 193$ nm. The results show a peak ratio of 0.4 at 18 km. This result may be compared with LIDAR measurements[32] showing peaks of 0.1–1 occurring at altitudes of 15–20 km. However, the LIDAR measurements were made using a wavelength of 694 nm. If the experimental ratios are adjusted to correspond to 193 rm by simply accounting for the increase in Rayleigh cross section, they would be reduced by a factor of 46. However, because the dependence of the aerosol backscattering cross section on the wavelength is uncertain, these predictions are left uncorrected as a conservative estimate. As a consequence, the predicted uncertainty imposed by particle scattering at $\lambda = 193$ nm exceeds 1% for all altitudes up to 50 km, while for $\lambda = 266$ nm it will exceed 1% at all altitudes up to 59 km because the Rayleigh signal is smaller.

Overall Signal-to-Noise Ratio Evaluation

To evaluate the SNR defined by Eq. (1), the total Rayleigh signal accumulated during a measurement interval in which

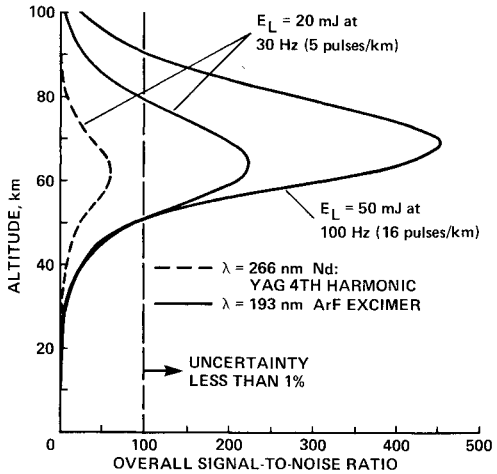

Fig. 4 Variations of the signal-to-noise ratio with altitude for a spatial resolution of 1 km.

n_{pulse} single-pulse signals are summed may be computed from Eq. (5) with corrections to account for the truncated signal-integration period. The uncertainty associated with photon-statistical noise can then be determined from the fundamental relation for a Poisson-statistical process that describes all photon statistics.[33] The resulting rms noise amplitude is

$$N_{phot} = [n_{pulse}(S_{Ray} + S_{part} + S_{solar})]^{1/2} \quad (12)$$

The overall measurement uncertainty is the sum of contributions from the photon-statistical noise, which includes the particle scattering signal, and the uncertainty in the determination of density from the total signal caused by particle scattering. Thus, the overall SNR may be estimated from

$$SNR = n_{pulse}S_{Ray}/(N_{phot} + n_{pulse}S_{part}) \quad (13)$$

The SNR values for three cases are plotted in Fig. 4 for altitudes up to 100 km. In one exmple, the performance of a frequency-quadrupled Nd:YAG laser and an ArF laser are compared when both lasers are operated at a single-pulse energy of 20 mJ and a repetition rate of 30 Hz. This comparison represents the case where both lasers are expected to require a similar amount of electrical power, assuming they both have the same electrical efficiency. The average power is limited by the maximum value at which a commercial Nd:YAG laser can be operated at 266 nm. For a spatial resolution of 1 km and flight speed of 6 km/s, the 30 Hz repetition rate allows signals from five laser pulses to be summed.

As Fig. 4 shows, the performance of currently available Nd:YAG lasers is not adequate for this application and a significant improvement in average power would have to be achieved to make it adequate. The SNR at all altitudes is lower for $\lambda = 266$ nm primarily because of the smaller Rayleigh cross section. Furthermore, the larger solar background contribution to noise at 266 nm reduces the SNR by about a factor of two.

On the other hand, the ArF laser operating at the same accumulated energy, but with a shorter wavelength, is clearly capable of meeting the measurement goals. Moreover, the ArF laser can also be operated at a significantly higher average power with little loss in reliability and possibly without a major increase in size and weight. For example, operation at 50 mJ and 100 Hz can now be obtained from most commercial excimer lasers, which corresponds to an eightfold increase in accumulated pulse energy along the 1 km flight-path interval. The resulting improvement in SNR and the extension of the altitude range is shown in Fig. 4.

From the results of these calculations, the most attractive choice for this application is an ArF laser that is capable of average powers approaching 5 W. Only the increased requirements for electrical power bring its selection into question. However, adequate electrical power is available on the Shuttle and little of it is in use during entry.

Laboratory Experiments

Stratosphere Simulator Facility

A principal aspect of this study is the experimental verification of the concept at conditions that reproduce the optical conditions expected in flight. To that end, a Stratosphere Simulator Facility was constructed specifically to demonstrate the capability of a representative instrument system and its associated electronics to obtain the expected signal levels, to achieve a linear signal variation with density, and to demonstrate signal-to-noise ratios near the predicted values. Except for the indefinite effects of solar background radiation and particle scattering, such a demonstration is sufficient to verify the predicted performance capabilities shown in Fig. 4 and to allow the confident specification of flight instrumentation.

The simulator facility was a 21-m-long vacuum vessel with an inside diameter of 60 cm. One end flange had an optical replica of the crew hatch window mounted in it, including three panes having the identical material, spacings, apertures, and thicknesses as the Shuttle window. The vessel could be pumped to any pressure over the range from 1 atm to below 10^{-5} Torr, thereby simulating atmosphere densities at all altitudes up to 125 km. During scattering measurements, the vessel was isolated from its pumps and the pressure was observed to remain constant to insure that no pump vapors or outgassing from the vessel walls contributed to the Rayleigh signals.

Laser Performance

The laser used for the verification experiments was a Questek (model 2260) ArF system with unstable resonator optics. It served only as a laboratory demonstration device and was not designed with a minimum size and weight. In one series of tests with the laser operating at 50 mJ/pulse and 100 Hz (thereby giving an average power of 5 W), it required 2.5 kW of electrical power (3.6 kVA and a power factor of 0.70) from a single-phase 208 V source. The laser was operated for 45 min at those conditions using a single gas fill with no gas purification or addition. These results demonstrate that an ArF laser can operate unattended over the duration of a Shuttle entry.

At an average laser power of 0.6 W, which was obtained with a pulse energy of 20 mJ at 30 Hz, the laser required 1.1 kW (1.6 kVA) of electrical power. However, at this condition the laser is 3.6 times less efficient than it is at 50 mJ/pulse and it is operating below its recommended minimum pulse energy. Therefore, a laser designed for this lower average laser power may require less than 1.1 kW of electrical power. On the other hand, the minimum electrical power required by the idling power supply with no high-voltage discharge was 350 W. These results suggest that the minimum electrical power required for any laser in this performance range can be expected to approach 1 kW.

Signal Background and Linearity

The Rayleigh signal following each laser pulse was detected using a Hamamatsu R2083Q PMT. Its nominal characteristics and those of the bandpass filter are given in Table 2. A reference signal, which was used to normalize the Rayleigh signal, was obtained with a Hamamatsu R1193U-02 photodiode that detected an attenuated fraction of the entire laser beam cross section. Both signals were integrated using a Stanford Research Systems SR250 boxcar averager. The Rayleigh signal waveform was integrated over a gate period of

80 ns, starting just prior to its initial rise. A much larger signal pulse, owing to the laser light reflected from the far end of the vacuum vessel, arrived after 140 ns and did not affect the Rayleigh-signal integral during the gate period. The integrated reference signal was proportional to the total pulse energy. Both the Rayleigh and reference integrals for each laser pulse were digitized with 12 bit resolution and transferred via an IEEE-488 GPIB interface to an IBM-AT computer where their ratio was computed. At each test condition, data sets for 2000 pulses were stored. Their average ratio and its standard deviation were subsequently computed. The combination of digitizing and normalizing processes limited the resolution of the normalized Rayleigh integral to 0.1% of full scale.

The variation of the normalized Rayleigh integral (NRI) signal with density was evaluated by varying the vessel pressure. At pressures below 10^{-2} Torr, the NRI signal was entirely dominated by background scattering of laser light from the vessel walls. The background came from highly divergent side lobes on the horizontal transverse axis of the laser beam and were the consequence of amplified internal reflections from the electrode rails in the laser. Although the effects of the side lobes were reduced using external spatial filtering of the beam, the background scattering caused by them could not be entirely eliminated. However, when the average background contribution measured in a fully evacuated vessel was subtracted from the average total NRI signals obtained at pressures above 10^{-2} Torr, the Rayleigh signal variation was linear with vessel pressure within the resolution of the measurement system. Such corrections would not be necessary in the flight application where no vessel walls are present.

At vessel pressures greater than 30 Torr, a reduction of the average NRI signal below that for a linear variation was observed. Thsi effect occurred in air, but not in nitrogen, and is the consequence of absorption of the laser beam by oxygen. However, a vessel pressure of 30 Torr corresponds to an equivalent density altitude of 24 km, which is much lower than the minimum altitudes at which this technique is applicable. Hence, in the altitude range of interest, absorption of the laser beam by oxygen will have no effect on the linearity of the signal variation with density.

Signal-to-Noise Ratios

The SNR for a single laser pulse is accurately determined by the ratio of the average NRI signal and its standard deviation for 2000 pulses. The experimental results are shown in Fig. 5 for the relevant range of vessel pressures. The equivalent density altitude that corresponds to each vessel pressure is also indicated. The laser was located 5 m from the photodetection electronics and operated at 20 Hz. The energy per pulse at the entrance window to the vessel was 10 mJ. The symbols represent measurements made with various PMT gains. They were adjusted to keep the signal within the range dictated by the maximum anode current at which the PMT is linear and the lowest signal that is accurately resolved by the digital processing. The error bars on the symbols represent the uncertainty owing to the digital resolution of the entire data reduction process at each condition.

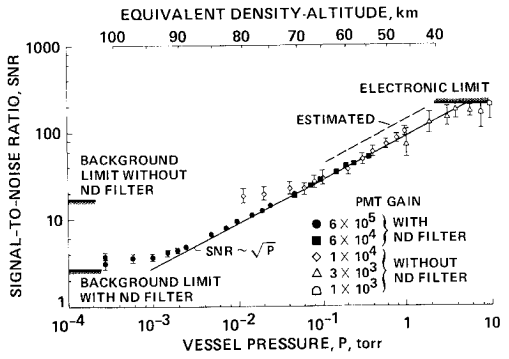

Fig. 5 Experimental and estimated signal-to-noise ratios in the Stratosphere Simulator Facility using an ArF laser operating at a wavelength of 193 nm and a pulse energy of 10 mJ (SNR data correspond to a single-pulse values derived from 2000 pulse averages).

The open symbols in Fig. 5 represent measurements made without any additional filters in the optical system. Above 0.1 Torr, they show the data to follow a line with a slope of ½ on this log-log plot, as it should if the noise is limited mainly by photon statistics according to Eq. (12). However, below 0.1 Torr, the SNR departs from the line as the average NRI approaches the lower limit caused by the background. Figure 5 also shows an electronic upper limit owing to the minimum noise that can be observed with the digital resolution in use.

Since the SNR data that are not significantly affected by background scattering behave according to Eq. (12), the performance of the system at pressures lower than the minimum allowed by the background can be simulated by placing a neutral density (ND) filter over the face of the PMT. It attenuates the background and reduces the Rayleigh signal to that corresponding to a lower pressure, while having no effect on electrical noise sources such as radio frequency interference (RFI) from the laser. Data taken with the ND filter are represented in Fig. 5 by the closed symbols. To calibrate the effective attenuation of the ND filter, the equivalent pressures were determined by using the decrease in SNR of the background signal measured in a fully evacuated vessel. The data taken with the ND filter were then associated with their equivalent pressure without further adjustment. The results merge with the unfiltered data, as expected, and provide an extension of the results over the full pressure range of interest.

A line showing the estimated SNR for the experimental conditions is also included in Fig. 5. It was calculated using the nominal parameters of each component in the system in the same manner used for the flight performance predictions. Its agreement with the experimental data is well within the combined uncertainty associated with those parameters. This result, taken in combination with the indication that the SNR data are limited primarily by photon-statistical noise, suggests that the experimental photon flux and the collection efficiency of the photodetection system are also in agreement with predictions. Thus, these results provide confidence that the performance estimates of the flight instrument shown in Fig. 4 are reasonable expectations.

Summary

An instrument system based on the use of Rayleigh scattering from an ArF laser is shown to be capable of providing direct measurements of atmospheric density during Space Shuttle entry with an uncertainty of less than 1% and with a spatial resolution of 1 km, over an altitude range of 50–90 km. Measurements at higher altitudes to 100 km, which extend into the low-density flow regime of the Shuttle, can also be obtained, but with greater uncertainties and lower spatial resolution.

The ultraviolet wavelength of 193 nm from the ArF excimer laser is shown to be the most favorable choice for this application because of the larger Rayleigh signal and the lower solar background that occur at shorter wavelengths. For comparison, a frequency-quadrupled Nd:YAG laser operating at 266 nm is also considered and shown not to be adequate for this application because of the loss of performance owing to the longer wavelength.

The primary parameter that characterizes the laser performance for this application is its average power. An ArF laser operating at an average power of 0.6 W is shown to be adequate for providing the required measurements. However, the performance of the system can be enhanced considerably by using a readily available laser with an average power of 5 W.

The vehicle utilities required to support an ArF laser operating at 0.6–5 W have been implied from tests using a commercial laser. The results show that the required electrical power is expected to be in the range of 1–2.5 kW. In addition, the laser with its power supply and gas supply could weigh up to 300 kg and may require liquid coolant at flow rates up to 4 l/min.

Experimental measurements were performed in a simulator facility at conditions duplicating the flight environment. They confirmed the ability of an instrument system that is assembled from commercially available equipment to meet the specified performance requirements. The experimental results demonstrated the achievement of signal-to-noise ratios that were at the predicted values and were limited primarily by photon statistics. From these results, the design requirements of a flight system can be specified with confidence.

Acknowledgment

The author is grateful to Francis X. Hurley, former NASA Deputy Chief Scientist, whose advocacy made this project possible, to Frank P. Scholz of Rockwell International for many helpful discussions, and to Bruce Banfield of NASA Ames for his assistance in the mechanical design of the Stratosphere Simulator Facility.

References

[1] *U.S. Standard Atmosphere, 1976*, National Oceanographic and Atmospheric Administration, NASA, U.S. Air Force, Rept. NOAA-S/T 76-1562, 1976.

[2] Hines, C. O., "Internal Atmospheric Gravity Waves at Ionospheric Heights," *Canadian Journal of Physics,* Vol. 38, Nov. 1960, pp. 1441–1481.

[3] Lindzen, R. S., "Turbulence and Stress Owing to Gravity Wave and Tidal Brakedown," *Journal of Geophysical Research,* Vol. 86, Oct. 1981, pp. 9707–9714.

[4] Rastogi, P. K. and Bowhill, S. A., "Scattering of Radio Waves from the Mesosphere—2. Evidence for Intermittent Mesosphere Turbulence," *Journal of Atmospheric and Terrestrial Physics,* Vol. 38, 1976, pp. 449–462.

[5] Findley, J. T., Kelly, G. M., and Troutman, P. A., "Final Report—Shuttle Derived Atmosphere Density Model (Parts 1 and 2)," NASA CR 171824, Dec. 1984.

[6] Blanchard, R. C. and Rutherford, J. F., "Shuttle Orbiter High Resolution Accelerometer Package Experiment: Preliminary Flight Results," *Journal of Spacecraft and Rockets,* Vol. 22, July–Aug. 1985, pp. 474–480.

[7] Price, J. M. and Blanchard, R. C., "Determination of Atmospheric Properties for STS-1 Aerothermodynamic Investigations," AIAA Paper 81-2430, Nov. 1981.

[8] Compton, H., Findley, J., Kelly, G., and Heck, M., "Shuttle (STS-1) Entry Trajectory Reconstruction," AIAA paper 81-2459, Nov. 1981.

[9] Siemers, P. M. III, Wolf, H., and Flanagan, P. F., "Shuttle Entry Air Data System Concepts Applied to Space Shuttle Orbiter Flight Pressure Data to Determine Air Data—STS 1-4," AIAA Paper 83-0118, Jan. 1983.

[10] Pruett, D. C., Wolf, H., Heck, M. L., and Siemers, P. M. III, "Innovative Air Data System for the Space Shuttle Orbiter," *Journal of Spacecraft and Rockets,* Vol. 20, Jan.–Feb. 1983, pp. 61–69.

[11] Blanchard, R. C., Duckett, R., and Hinson, E. W., "The Shuttle Upper Atmosphere Mass Spectrometer Experiment," *Journal of Spacecraft and Rockets,* Vol. 21, March–April 1984, pp. 202–208.

[12] Siemers, P. M. III, NASA Langley Research Center, private communication.

[13] McKenzie, R.L., "A Method of Atmospheric Density Measurement During Shuttle Entry Using UV Laser Rayleigh Scattering," AIAA Paper 87-1530, June 1987.

[14] Samson, J. A. R., "On the Measurement of Rayleigh Scattering," *Journal of Quantitative Spectroscopy and Radiative Transfer,* Vol. 9, 1969, pp. 875–879.

[15] Shardanand and Rao, A.D.P., "Absolute Rayleigh Scattering Cross Sections of Gases and Freons of Strateospheric Interest in the Visible and Ultraviolet Regions," NASA TN D-8442, March 1977.

[16] Penndorf, R., "Tables of the Refractive Index for Standard Air and the Rayleigh Scattering Coefficient for the Spectral Region between 0.2 and 20.0 μ and Their Application to Atmospheric Optics," *Journal of the Optical Society of America,* Vol. 47, Feb. 1957, pp. 176–182.

[17] Edlen, B., "The Dispersion of Standard Air," *Journal of the Optical Society of America,* Vol. 43, May 1953, pp. 339–344.

[18] Taylor, D. J., Los Alamos National Laboratory, Private communication.

[19] Lewis, B. R., Berzins, L., Carver, J. H., and Givson, S. T., "Rotational Variation of Predissociation Linewidth in the Schumann-Runge Bands of 16_{O_2}," *Journal of the Quantitative Spectroscopy and Radiative Transfer,* Vol. 36, No. 3, 1986, pp. 187–207.

[20] Lewis, B. R., Berzins, L., and Carver, J. H., "Oscillator Strengths for the Schumann-Runge Bands of 16_{O_2}," *Journal of the Quantitative Spectroscopy and Radiative Transfer,* Vol. 36, No. 3, 1986, pp. 209–232.

[21] Prabhu, D. K., and Tannehill, J. C., "Numerical Solution of Space Shuttle Orbiter Flowfield Including Real-Gas Effects," *Journal of Spacecraft and Rockets,* Vol. 23, May–June 1986, pp. 264–272.

[22] Chaussee, D. J., NASA Ames Research Center, private communication.

[23] Goodrich, W D., NASA Johnson Space Center, private communication.

[24] *Laser Focus Buyers' Guide, 1987*, Pennwell Publishing, Littleton, MA, 1987.

[25] Thekaekara, M. P., "Extraterrestrial Solar Spectrum, 3000-6100 A at 1-A Intervals," *Applied Optics,* Vol. 13, March 1974, pp. 518–522.

[26] Plass, G. N. and Kattawar, G. W., "Calculations of Reflected and Transmitted Radiance for Earth's Atmosphere," *Applied Optics,* Vol. 7, June 1968, pp. 1129–1135.

[27] Van de Hulst, H. C., *Light Scattering by Small Particles,* Wiley, New York, 1957.

[28] McClatchey, R. A., Fenn, R. W., Selby, J. E. A., Volz, F. E., and Garing, J. S., "Optical Properties of the Atmosphere," *Handbook of Optics,* McGraw-Hill, New York, 1988, Sec. 14.

[29] Volz, F. E., "Infrared Refractive Index of Atmospheric Aerosol Substances," *Applied Optics,* Vol. 11, April 1972, p. 755.

[30] Deirmendjian, D., "Scattering and Polarization Properties of Water Clouds and Hazes in the Visible and Infrared," *Applied Optics,* Vol. 3, Feb. 1964, pp. 187–196.

[31] Hunten, D. M., Turco, R. P., and Toon, O. B., "Smoke and Dust Particles of Meteoric Origin in the Mesosphere and Stratosphere," *Journal of the Atmospheric Sciences,* Vol. 37, June 1980, pp. 1342–1357.

[32] Whitten, R. C. (ed.), "The Stratospheric Aerosol Layer," *Topics in Current Physics,* Vol. 28, Springer-Verlag, New York, 1982.

[33] Kingston, R. H., *Detection of Optical and Infrared Radiation,* Springer-Verlag, New York, 1978.